Malaysian Journal of Analytical Sciences (MJAS)
Published by Malaysian Analytical Sciences Society

POLYPHENOL-MEDIATED GREEN SYNTHESIS OF ZINC OXIDE AND THEIR ANTIBACTERIAL PROPERTIES: A NOVEL SIZE-CONTROLLED APPROACH

(Sintesis Hijau dengan Mediasi Polifenol dan Ciri Antibakteria Zink Oksida: Pendekatan Kawalan Saiz Baharu)

Neo Zhi Zing[1], Balkis A. Talip[1]*, Soon Chin Fhong[2], Ainun Rahmahwati Ainuddin[3], Hatijah Basri[1]

[1]Faculty of Applied Sciences and Technology,
[2]Microelectronics and Nanotechnology-Shamsuddin Research Centre, Faculty of Electrical and Electronics Engineering
[3]Nano Structure and Surface Modification (NANOSURF), Faculty of Mechanical Engineering and Manufacturing
Universiti Tun Hussein Onn Malaysia, 86400 Parit Raja, Batu Pahat, Johor, Malaysia

**Corresponding author: balkis@uthm.edu.my*

Received: 15 March 2022 ; Accepted: 18 May 2022 ; Published: 25 August 2022

Abstract

The concept of feasibility in green synthesis of zinc oxide (ZnO) nanoparticles has been discussed in many studies. However, size control using volume of plant extracts undermines the process upscaling potential. This study is aimed at improving the repeatability and reproducibility of green synthesis of ZnO by controlling total phenolic content of plant extracts. Leaf extracts of *Camellia sinensis, Manilkara zapota* and *Elaeis guineensis* were incorporated at gallic acid equivalent of 100 mgg^{-1} to synthesize ZnO. The phytochemical profile of plant extracts and physical properties of ZnO were determined. In addition, antibacterial activity of ZnO against *Escherichia coli* and *Staphylococcus aureus* was examined. Consistency in particle sizes of ZnO has justified the feasibility of using total phenolic content for size control. Under neutral pH, role of phytochemicals as chelating agents predominated. Under basic condition, complex phytochemicals demonstrated structure-directing effect on ZnO microparticles. The antibacterial strength of ZnO has been reduced by 16 times with reduction in particle size. Meanwhile, the incorporation of phytochemicals enhanced antibacterial activity of ZnO by fourfold. This study proposed that particle size and morphology of ZnO could be controlled through manipulation of total phenolic content of plant extracts and the reaction pH of green synthesis.

Keywords: green synthesis, polyphenol, zinc oxide, size control

Abstrak

Konsep dalam kebolehlaksanaan proses sintesis hijau terhadap nanopartikel zink oksida (ZnO) telah diperjelaskan dalam pelbagai kajian. Namun begitu, kawalan saiz menggunakan isipadu ekstrak tumbuhan menjejaskan potensi dalam meningkatkan skala proses. Kajian ini bertujuan untuk meningkatkan kebolehulangan sintesis hijau ZnO dengan mengawal jumlah kandungan fenolik ekstrak tumbuhan yang digabungkan. Ekstrak daun *Camellia sinensis*, *Manilkara zapota* dan *Elaeis guineensis* telah dicampurkan pada persamaan asid gallik sebanyak 100 mgg^{-1} untuk menghasilkan ZnO. Profil fitokimia ekstrak tumbuhan dan sifat fizikal ZnO telah ditentukan. Di samping itu, aktiviti antibakteria ZnO terhadap *Escherichia coli* dan *Staphylococcus aureus* telah diperiksa. Ketekalan dalam saiz partikel ZnO menjustifikasikan kebolehlaksaan penggunaan jumlah kandungan fenolik untuk kawalan saiz

dalam sintesis hijau. Di bawah pH neutral, peranan fitokimia sebagai agen pengkelat berdominasi. Di bawah keadaan alkali, fitokimia kompleks menunjukkan kesan pengarahan struktur pada mikropartikel ZnO. Kekuatan antibakteria ZnO berkurangan sebanyak 16 kali ganda dengan pengurangan saiz partikel. Sementara itu, penggunaan fitokimia dalam proses sintesis telah meningkatkan aktiviti antibakteria ZnO sebanyak 4 kali ganda. Kajian ini mencadangkan bahawa saiz partikel dan morfologi ZnO boleh dikawal melalui manipulasi jumlah kandungan fenolik ekstrak tumbuhan dan pH tindak balas sintesis hijau.

Kata kunci: sintesis hijau, polifenol, zink oksida, kawalan saiz

Introduction

Nanotechnology is an extensively researched field with an anticipated global market share of approximately 55 million dollars by 2022 [1]. Nanomaterials are categorized depending on their compositions, which includes carbon, organic, inorganic, and composite compounds [2]. Metal oxide nanoparticles fall under composite-based nanomaterials. Metal oxide nanoparticles are synthesized in the laboratory via physical and chemical methods [3,4]. However, the upscaling of two methods suffers from the limitations due to the need for sophisticated technology, high-energy consumption, and the use of toxic chemicals [5]. Recent trends in nano synthesis reveal a growing interest in the utilization of biological materials to react with metal precursors under regulated conditions [6, 7]. The terms "green synthesis" and "biosynthesis" are used interchangeably to describe the synthesis of nanoparticles using biological components derived from bacteria, fungi, algae, and plants [4]. Green synthesis that utilizes plant extracts as the bioreductants is a sustainable route since phytochemicals can be extracted from any plant parts [8]. Due to the essential starting materials which are metal precursors, plant extracts, and water, green synthesis of metal oxide nanoparticles are both cost-effective and environmentally friendly [3, 4]. Apart from being reducing and chelating agents, phytochemicals can act as capping agents to regulate the morphology and particle size of nanoparticles [3, 4].

Zinc oxide (ZnO) nanoparticles have gained attention for a wide range of applications due to their distinctive physical and chemical properties. They have been described as a photocatalytic adsorbent for water treatment, gas sensors, solar cells, and an active component in cosmetics [9]. Meanwhile, the biocidal action of ZnO nanoparticles against harmful microbes has piqued the interest of researchers in commercializing them as preservatives and biocidal products [10, 11]. The versatility of ZnO nanoparticles has prompted the development of a green synthetic pathway that incorporates different plant extracts. However, the incorporation of plant extracts is expressed in weight, volume, or percentage, with no quantitative information on the phytochemicals present in the reaction. Xu et al. [12] emphasized that plant extract concentration is one of the major manipulating factors in the green synthesis of ZnO nanoparticles. Even though a trend was observed in which the size of nanoparticles decreased as the concentration of plant extract used increased, the method was not replicable because the unit employed to express the incorporation of plant extract was empirical. Lack of information in reaction mechanisms also limit the effort in advancing green synthesis. It is ideal for controlling the biologically active compounds present in the extracts. Polyphenols are the most prevalent phytochemicals in the plant kingdom [13]. They are regarded as a marker group for the quality evaluation of medicinal plants due to their significant roles in the biological activity of extracts [14]. In fact, a study has been carried out to determine the roles of isolated phenolic acids in the green synthesis of metal nanoparticles [15].

This work is fundamental research undertaken with the goal of improving the repeatability and reproducibility of green synthesis for ZnO size control. This study was also intended to elucidate the reaction mechanisms of the green synthesis of ZnO.

Materials and Methods

Materials

Commercial *Camellia sinensis* (black tea leaves) were purchased from local market while leaves of *Manilkara zapota* (sapodilla) and *Elaies guineensis* (oil palm) were obtained from local plantation. Folin-Ciocalteu (FC) reagent, sodium carbonate (Na_2CO_3), benzene, ammonia solution, methanol, aluminium chloride

($AlCl_3$), chloroform, sulphuric acid (H_2SO_4), and zinc oxide (ZnO) were bought from Merck (Darmstadt, Germany). Gallic acid, sodium hydroxide (NaOH), zinc nitrate hexahydrate [$Zn(NO_3)_2.6H_2O$], and resazurin sodium salt were purchased from Sigma-Aldrich Co. (St. Louis, MO, USA). Wagner's solution was purchased from Avondale Laboratories (Banbury, England). Meanwhile, hydrochloric acid (HCl) and ferric chloride ($FeCl_3$) were obtained from QRëC (Selangor, Malaysia) and R&M Chemicals (Selangor, Malaysia) respectively.

Bacterial culture of *Escherichia coli* ATCC 8739 and *Staphylococcus aureus* ATCC 25923 were purchased from Remel Europe (Dartford, England). The McFarland Standard was supplied by ThermoFisher Scientific (Massachusetts, USA). Mueller Hinton Broth (MHB) and Mueller Hinton Agar (MHA) were from Condalab (Madrid, Spain). Meanwhile, oxacillin sodium salt monohydrate and ampicillin sodium salt were obtained from HiMedia Laboratories (Mumbai, India).

Aqueous extraction of phytochemicals

Commercial black tea leaves were used as-is. Fresh *chikoo* leaves and oil palm leaves were cleaned with tap water and dried overnight in convection oven at 65 ˚C (UFE500, Memmert GmbH + Co.KG, Germany). Dried plant leaves were ground using kitchen blender. Aqueous extraction method of Mercado-Mercado et al. [16] was employed with modification. Samples were decocted in deionized water through double boil method at 85 ˚C for 15 min. The decoction ratio was 1 part ground leaves to 10 parts deionized water. Decocted samples were filtered through muslin cloth. Then, the aqueous extracts were centrifuged at 1,500 rpm for 1 min at room temperature (Centrifuge 5804 R, Eppendorf, Germany). The aqueous extracts were filtered through Whatman No. 1 filter paper. Then, the crude plant extracts were dried in convection oven at 65 ˚C (UFE500). Dried crude plant extracts were ground into fine powder using pestle and mortar. Sample codes for the crude plant extracts were BTLE (black tea leaf extract), CLE (*chikoo* leaf extract) and OPLE (oil palm leaf extract).

Determination of total phenolic content

Folin-Ciocalteu assay was performed with reference to method of Dudonné et al. [17]. The reaction began by mixing 400 µL aqueous sample solution with 2.0 mL of FC reagent (diluted to 10-fold in deionized water). After 5 minutes, 1.6 mL of 7.5% Na_2CO_3 solution was added into the mixture and mixed thoroughly. The mixture was allowed to react for 1 h at room temperature. Absorbance value was measured at 765 nm using UV-Vis spectrophotometer (Spectrophotometer T60 U, PG Instruments Ltd., UK). All tests were performed at triplicates. The calibration curve was plotted using aqueous solution of gallic acid.

Identification of organic compounds

The organic compounds present in crude plant extracts were identified using Attenuated Total Reflection - Fourier transform infrared (ATR-FTIR) spectroscope (Spectrum Two, Perkin Elmer, USA). The FTIR spectra of the extracts were examined by placing powder of crude plant extract directly onto the crystal plate of ATR-FTIR spectroscope. The measurement was taken in the range of 4000-400 cm^{-1} with a resolution of 4 cm^{-1}.

Screening for phytochemicals

Aqueous solutions of BTLE, CLE and OPLE were prepared at concentration of 1 $mgmL^{-1}$ for the screening of phytochemicals. The aqueous plant extracts were screened for the presence of alkaloids, anthraquinones, flavonoids, saponins, steroids, tannins, and terpenoids.

Wagner's test was used to determine the presence of alkaloids. Few drops of Wagner's solution were added to the aqueous plant extracts. Formation of brown precipitate indicated the presence of alkaloid [18]. The presence of anthraquinones was tested by adding 10 mL benzene to 5 mL aqueous plant extracts. Then, 10 mL 10% ammonia solution was added to the mixture. The mixture was shaken vigorously. Presence of anthraquinones was indicated by pink, violet or red colour solution [19].

The presence of flavonoids was examined with Shinoda's test, aluminium chloride test and alkaline reagent test. In Shinoda's test, 4 mL aqueous plant

extract was mixed with 1.5 mL 50% methanol. Magnesium metal was added to the mixture followed by the addition of few drops of fuming HCl. Changes of colour of mixture to red indicated the presence of flavonoids [20]. In aluminium chloride test, 5 mL aqueous plant extract was added with 1 mL 1% $AlCl_3$ solution. The solution was shaken vigorously. Presence of yellow precipitates indicated presence of flavonoids [21]. Meanwhile, alkaline reagent test was performed by mixing 2 mL 2.0% NaOH solution with aqueous plant extract. In the presence of flavonoids, concentrated yellow solution would turn colourless with addition of 2 drops of 2 M HCl [19].

The presence of saponins in plant extracts was examined using method of El Aziz et al. [22] with modifications. Five millilitres (5 mL) aqueous plant extract was vortexed for 2 min. Presence of saponins was confirmed by persistent appearance of foam lasting for at least 15 min. Salkowski's test was performed to confirm the presence of steroids. Two millilitres (2 mL) chloroform and 2 mL concentrated H_2SO_4 were added to 5 mL aqueous plant extract. Red colouration in lower chloroform layer indicated presence of steroids [19]. Presence of tannins was indicated by greenish black colouration formed from reaction between 5 mL aqueous plant extract and 1 mL 5% $FeCl_3$ solution [23]. Screening for the presence of terpenoids commenced by mixing 2.5 mL aqueous plant extract with 2.5 mL chloroform. The mixture was evaporated to dryness. Then, 3 mL concentrated H_2SO_4 was added and boiled for 10 min. A grey solution would form in the presence of terpenoids [21].

Synthesis of ZnO

Synthesis method of Top et al. [24] was adapted with modification. The combinations of reaction mixture and sample codes are summarized in Table 1.

Table 1. Combinations of reaction mixture and sample codes of zinc oxide

Reaction Mixture	Molar Ratio of $Zn(NO_3)_2.6H_2O$ to NaOH	Sample Codes of ZnO with Reference to Incorporated Crude Plant Extract		
		BTLE	CLE	OPLE
B	1.0 : 2.0	$ZnO_{BTLE(B)}$	$ZnO_{CLE(B)}$	$ZnO_{OPLE(B)}$
C	1.0 : 1.8	$ZnO_{BTLE(C)}$	$ZnO_{CLE(C)}$	$ZnO_{OPLE(C)}$
D	1.0 : 1.6	$ZnO_{BTLE(D)}$	$ZnO_{CLE(D)}$	$ZnO_{OPLE(D)}$
E	1.0 : 1.4	$ZnO_{BTLE(E)}$	$ZnO_{CLE(E)}$	$ZnO_{OPLE(E)}$
F	1.0 : 1.2	$ZnO_{BTLE(F)}$	$ZnO_{CLE(F)}$	$ZnO_{OPLE(F)}$
G	1.0 : 1.0	$ZnO_{BTLE(G)}$	$ZnO_{CLE(G)}$	$ZnO_{OPLE(G)}$
Control sample				
A	1.0 : 2.0		$ZnO_{control(A)}$	
H	1.0 : 1.0		$ZnO_{control(H)}$	

The pH of reaction mixture was measured using pH meter (pH 700, Eutech Instrument, USA). The concentration of crude plant extracts employed for green synthesis was computed from volume of gallic acid equivalent (GAE) based on the results of total phenolic content (TPC) obtained prior to synthesis. All crude plant extracts were added at 100 mg GAE g^{-1}. The reaction mixtures were incubated in incubator shaker at 60 ˚C for 1 hour with constant agitation (KS 4000 i control, IKA, Germany). After 1 hour, the precipitates were collected through centrifugation followed by twice washing with deionized water (Centrifuge 5804 R). The collected precipitates were dried in convection oven at 60 ˚C for 24 hours (UFE500). Calcination was

conducted at 500 ˚C for 3 hours (ELF 11/14 Chamber Furnace, Carbolite Gero, UK). Each synthesis pathway was performed in triplicates. Representative samples were prepared for further analysis.

Determination of minimum inhibitory concentration and minimum bactericidal concentration

The viability of *E. coli* and *S. aureus* under exposure to different concentrations of ZnO was determined through Resazurin Cell Viability Test using method by He et al. [25] with modification. Bacterial culture was grown in MHB and incubated in incubator shaker at 37 ˚C for 24 hours with constant agitation (KS 4000 i control). The overnight bacterial cells were suspended in sterilized 0.9 % saline solution and adjusted to 2.0 McFarland Standard and 3.0 McFarland Standard for *S. aureus* and *E. coli* respectively.

Samples of ZnO were suspended in sterilized distilled water at concentration of 8 $mgmL^{-1}$. The suspension was mixed thoroughly with vortex mixer for 1 min (MX-S, Dragon Laboratory Instruments Ltd., China). The samples of ZnO were deployed with twofold dilution at starting concentration of 8 $mgmL^{-1}$ for *S. aureus* and 16 $mgmL^{-1}$ for *E. coli*. To each well containing 100 µL ZnO suspension, 100 µL bacterial suspension and 20 µL 0.02% resazurin solution were added. Positive control (without ZnO samples) and negative control (without bacterial suspension) were included in each plate. The 96 well microtiter plate was incubated at 37 ˚C for 24 hours (INB500, Memmert GmbH + Co.KG, Germany). To compare effectiveness of ZnO samples and commercial antibiotics against the tested strains of bacteria, Resazurin Cell Viability Test was performed by employing ampicillin and oxacillin at starting concentration of 8 $mgmL^{-1}$ under the same protocol.

Colour changes were observed and recorded after incubation period. The lowest concentration of ZnO samples that inhibited visible growth of microorganisms after overnight incubation was considered the minimum inhibitory concentration (MIC). A loopful of aliquot from the MIC well was transferred and streaked on MHA. The streak plates were incubated at 37 ˚C for 24 hours. Viability of bacterial cells was observed after 24 hours for the determination of bactericidal or bacteriostatic properties at MIC of ZnO samples. All tests were conducted at triplicates.

Statistical analysis

The results of replicated tests were expressed as mean value with standard deviations. Comparison between means of independent groups was analysed by one-way analysis of variance (ANOVA) followed by Tukey's honestly significant difference (HSD) post hoc test ($p<0.05$). Correlation analysis was performed using Pearson's correlation coefficient (R) in bivariate linear correlations ($p<0.01$). All statistical analysis was computed using IBM SPSS Statistics 22.0.

Results and Discussion

Morphology, particle size and elemental composition of ZnO

The designed pathways resulted in the synthesis of nano- and microsized zinc oxide (ZnO). In the current study, ZnO particles smaller than 100 nm were referred to as ZnO nanoparticles, while those larger than this size limit were defined as ZnO microparticles. Table 2 summarizes the particle sizes of ZnO obtained from the study. Morphologies of ZnO nanoparticles and ZnO with defined microstructures are shown in Figure 1. Elemental analysis validated the purity of all samples.

Reaction mixtures E, F, and G with the incorporation of CLE and OPLE and reaction mixture G with the incorporation of BTLE were capable of producing ZnO nanoparticles. The irregularly shaped nano- and micro-particles agglomerated into microstructures with no defined morphology as the molar ratio of $Zn(NO_3)_2$ to NaOH increased. Zinc oxide microparticles in the shape of microflower were obtained using the reaction mixtures control(A), BTLE(B), and CLE(B), while ZnO in the shape of spheroid microstructure was obtained from reaction mixture OPLE(B). It is important to highlight that the morphologies and size ranges of $ZnO_{control(A)}$ and $ZnO_{control(H)}$ are similar to those of their respective green synthesis counterparts.

The particle sizes of ZnO decreased within the crude plant extract group in response to a reduction in the molar ratio of $Zn(NO_3)_2$ to NaOH and a simultaneous increase in the ratio of plant extracts used at a

concentration of 100 mg GAE g^{-1}. Likewise, standard errors, which represent the range of particle size distribution, decreased along with the trend. However, the sample of $ZnO_{CLE(G)}$ contained a heterogeneous mixture of nanoparticles and microparticles. As the condition was an isolated case that was not observed in other samples produced under the same conditions ($ZnO_{BTLE(G)}$, $ZnO_{OPLE(G)}$, $ZnO_{control(H)}$), particle size measurements were only performed on nanoparticles that were not arranged into microstructures.

Table 2. Particle sizes and morphologies of zinc oxide

Reaction Mixture	**Shape and Morphology**	**Particle Size, nm**		
		ZnO_{BTLE}	**ZnO_{CLE}**	**ZnO_{OPLE}**
B	Microflower (ZnO_{BTLE} and ZnO_{CLE}); spheroid (ZnO_{OPLE})	Length: 838.97 ± 195.97[a]; width: 608.80 ± 112.67[a]	Length: 1736.63 ± 405.47[b]; width: 885.43 ± 196.06[b]	Length: 943.30 ± 118.61[a]; width: 719.53 ± 176.59[a]
C	Agglomerated microparticles	214.02 ± 39.69[a]	317.68 ± 48.30[b]	217.40 ± 42.99[a]
D	Agglomerated microparticles	159.30 ± 46.92[a]	239.72 ± 48.63[b]	154.92 ± 42.59[a]
E	Agglomerated microparticles	149.33 ± 32.00[a]	92.55 ± 23.89[b]	81.15 ± 26.17[b]
F	Agglomerated microparticles	121.80 ± 32.02[a]	71.22 ± 21.65[b]	80.62 ± 27.37[b]
G	Nanoparticles	70.77 ± 21.74[a]	41.87 ± 15.52[b]	63.80 ± 21.33[a]
A	Microflower	Length: 1193.30 ± 193.31; width: 700.47 ± 145.09		
H	Nanoparticles	81.17 ± 21.02		
Analytical grade ZnO	Nanorods	Length: 196.80 ± 79.93; width: 81.20 ± 29.65		

[a,b] denote significant difference for data within row ($p<0.05$)

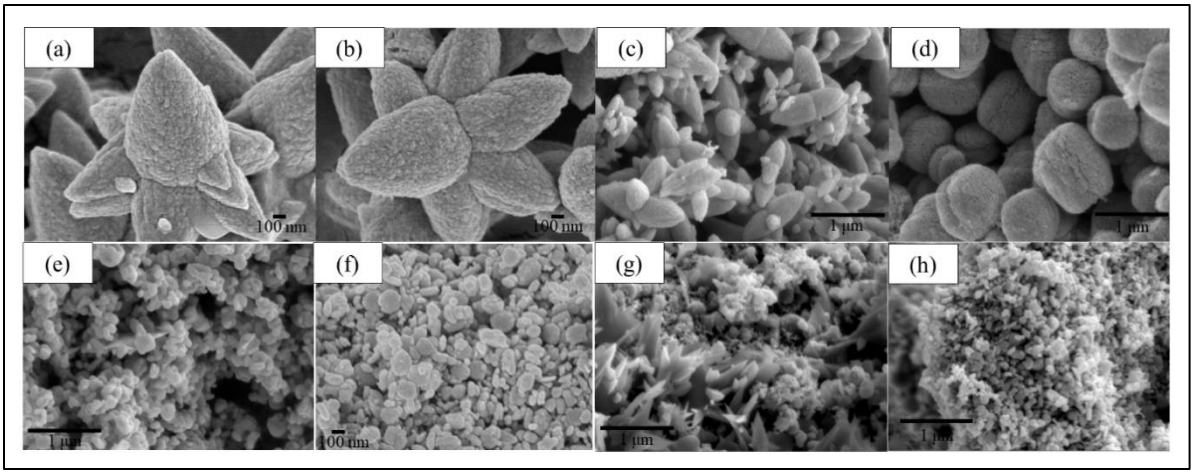

Figure 1. FESEM images of ZnO observed under magnification of 50,000x (a) $ZnO_{control(A)}$, (b) $ZnO_{BTLE(B)}$, (c) $ZnO_{CLE(B)}$, (d) $ZnO_{OPLE(B)}$, (e) $ZnO_{control(H)}$, (f) $ZnO_{BTLE(G)}$, (g) $ZnO_{CLE(G)}$, (h) $ZnO_{OPLE(G)}$

Meanwhile, particle sizes of ZnO were found to differ significantly (p <0.05) across the group of crude plant extracts. However, a statistically significant linear relationship with the trend in particle size reduction was observed for ZnO synthesized with the incorporation of crude extracts of black tea and oil palm leave (p <0.01). A positive linear relationship with a strong magnitude of association was observed (r=0.997). It is deduced that there is a potential in using the total phenolic content of plant extracts for size control of ZnO through the proposed pathway when different plant extracts are employed.

Moreover, the particle sizes of representative samples from the triplicate synthesis procedure showed no significant difference (p >0.05), implying that the synthesis pathway is repeatable. The designed protocol is feasible for size control in order to achieve consistency in the particle size of ZnO.

Phytochemical analysis of the crude plant extracts

The total phenolic content (TPC) of crude plant extracts differed significantly (p <0.05), with CLE containing the highest phenolic compounds (1.07 ± 0.13 mg GAE g^{-1}), followed by BTLE (0.87 ± 0.09 mg GAE g^{-1}) and OPLE (0.37 ± 0.10 mg GAE g^{-1}). During the green synthesis incorporation, significant differences in TPC of crude plant extracts had translated to significant weight differences. The OPLE was incorporated at the highest weight per volume.

A broad band recorded between 3650 and 3250 cm^{-1}, accompanied by the absorption bands between 1600 and 1300 cm^{-1} and 1200 and 1000 cm^{-1} indicated the presence of hydrogen bonds [26]. Grasel et al. [27] reported that bands in 3500 to 3100 cm^{-1} resulted from hydroxyl (–OH) group stretching, were common characteristics of polyphenolic compounds. The aromatic ring stretching group frequency was determined to be between 1615 and 1580 cm^{-1} [26, 28]. Absorption peaks around 2970-2950 cm^{-1} and 2880-2860 cm^{-1} were evidences of saturated aliphatic groups [28]. All tested plant extracts showed absorption peaks in the specified wavenumbers ranges except for alkanes (Figure 2). The spectra provided pieces of evidence for the presence of phenolic compounds with –OH and –COOH side chains in the samples.

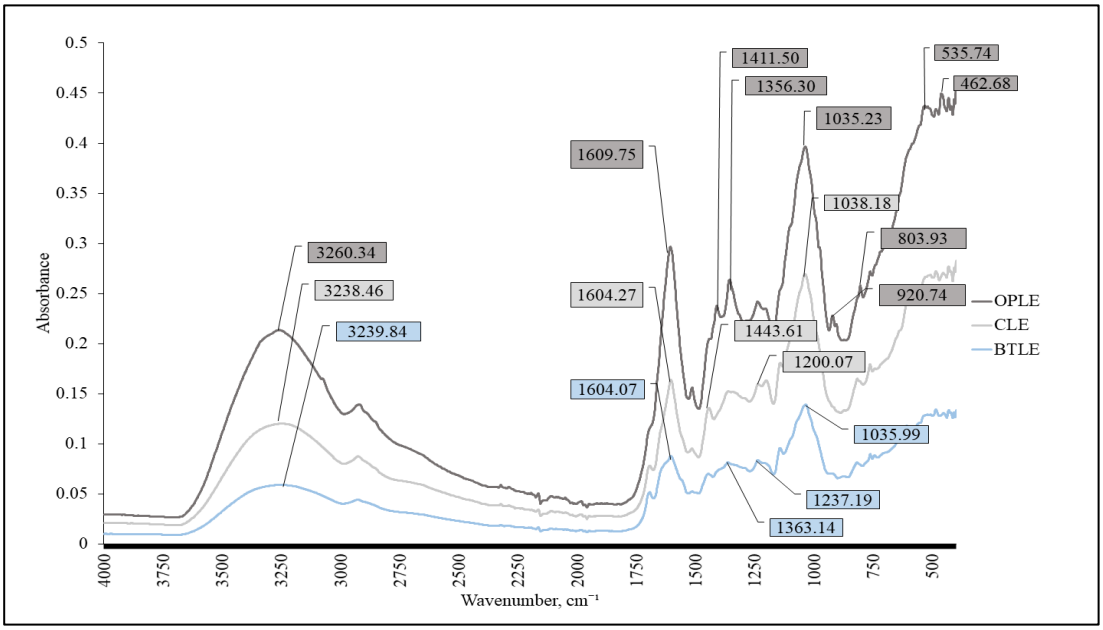

Figure 2. The crude plant extracts were composed primarily of phenolic compounds. OPLE registered the most number of peaks in the IR spectra. It is inferred to be composed of relatively more complex organic compounds compared to CLE and OPLE

Phytochemicals of OPLE were speculated to be larger organic molecules compared to those of BTLE and CLE. The presence of amine groups (C-N) were only observed in OPLE samples at 920.74 cm^{-1} and 535.74 cm^{-1}. Moreover, absorption bands less than 1000 cm^{-1} were only observed in OPLE. Bands at around 750-500 cm^{-1} were associated with alkenes =C-H bending [29]. The alkane C-C bending vibrations were manifested as absorption peak below 500 cm^{-1} [29]. In addition, the presence of absorption bands at wavenumbers less than 1000 cm^{-1} was claimed to be an indicator for the presence of isoprenoid [30,31]. The presence of isoprenoid in OPLE was speculated.

The phytochemical composition of plant extracts is summarized in Table 3. Oil palm leaf extract was the only crude plant extract that was screened positive for alkaloids. In addition, the absorption peaks at wavenumber 920.74 and 535.74 cm^{-1}, which were assigned to N-CH_3 symmetric stretching and C-N-CH_3 deformation of alkaloids [32], were observed in IR spectrum of OPLE. Although the IR fingerprint for isoprenoid was only observed in OPLE's IR spectrum, saponins, which is a form of polar isoprenoids, were found to be present in all crude extracts.

By combining the observations from the Folin-Ciocalteu assay and FTIR analyses, it was determined that all plant extracts were primarily composed of phenolic compounds. Overall, in comparison to both BTLE and CLE, OPLE contains relatively more complex phytochemicals, made up of phenolic compounds with hydroxyl, carboxyl, and amine groups. The complexity of phytochemicals in OPLE had contributed to the inconsistency in process output, in terms of morphologies of ZnO, across different crude plant extracts.

Table 3. Phytochemical compounds present in aqueous plant extracts

Phytochemical Compounds	**Type of Aqueous Plant Extract**		
	BTLE	**CLE**	**OPLE**
Alkaloids	-	-	+
Anthraquinones	-	-	-
Flavonoids			
- Shinoda' test	-	-	-
- Aluminium chloride test	-	-	-
- Alkaline reagent test	-	-	-
Saponins	+	+	+
Steroids	+	+	-
Tannins	+	+	+
Terpenoids	+	-	+

+ denotes present, - denotes absent

Effects of pH and concentration of plant extracts on the formation of ZnO

The pH of reaction mixtures did not differ significantly when the molar ratio of $Zn(NO_3)_2$ to NaOH was changed from 1.0:1.0 to 1.0:1.8 (p >0.05). The pH of the reaction mixtures was determined to be neutral (Table 4). However, significant difference was observed when the molar ratio of the reaction mixture was raised to 1.0:2.0 (p <0.05), where the pH increased to 11.44. It is worth noting that despite bearing no pH difference, a trend of particle size reduction was observed from reaction mixtures C to G. The trend was attributed to the additive effect of phytochemical capping properties, in addition to the size reduction effect of reaction pH

Table 4. The pH of reaction mixtures

Molar ratio of $Zn(NO_3)_2$ to NaOH	**pH**
1.0 : 2.0	11.44 ± 0.25^a
1.0 : 1.8	7.59 ± 0.24^b
1.0 : 1.6	7.46 ± 0.02^b
1.0 : 1.4	7.34 ± 0.03^b
1.0 : 1.2	7.23 ± 0.01^b
1.0 : 1.0	7.16 ± 0.03^b

[a,b] denote significant difference (p <0.05)

Studies showed that the degree of organization of ZnO nanoparticles increases with an increase in pH of reaction mixture [33, 34]. Meanwhile, studies in green synthesis of ZnO nanoparticles revealed that increasing the pH resulted in particle size increment despite the acclaimed function of plant extracts as capping agents [35-37].

The observations necessitate the answers to the following questions, 'Is the addition of base necessary in green synthesis?', 'Would the addition of base negate the effect or alter the role of plant extracts?' and 'What is the advantage of ZnO produced through green synthesis over the one produced through direct reaction between $Zn(NO_3)_2$ and NaOH when both exhibit the same morphology?'.

Proposed mechanisms for the green synthesis of ZnO nanoparticles

Plant extracts are widely accepted to act as reducing agents in green synthesis [38,39]. In the current work, no precipitation was observed when $Zn(NO_3)_2$ and plant extracts were used as the only process inputs. In fact, precipitation was observed upon mixing of NaOH and $Zn(NO_3)_2$ in the absence of phytochemicals. Additionally, it was observed that precipitates bearing the color of the incorporated plant extracts were produced following the addition of NaOH. Fine white ZnO powder was produced after calcination.

A review of recent studies reveals that all three pathways illustrated in Figure 3 are employed and classified as green synthesis. Pal et al. [7], Suresh et al. [38] and Sharmila et al. [40] implemented pathway B to produce ZnO nanoparticles, while Matinise et al. [41] adopted pathway C. Meanwhile, pathway A involves the addition of NaOH as an alkalizing agent or precipitating agent [42-44]. To elucidate the reaction mechanism, emphasis was made on the nature of divalent zinc (Zn^{2+}) ions and phytochemicals. Divalent zinc ion acts as an intermediate Lewis acid, which can interact with a wide range of ligand bases to form Zn complexes with up to six coordination numbers [45,46,47]. The nature of zinc relies on the redox potential and pH values, where it exists as hydrated zinc complexes in acidic conditions and as zinc hydroxo complexes in alkaline conditions [46].

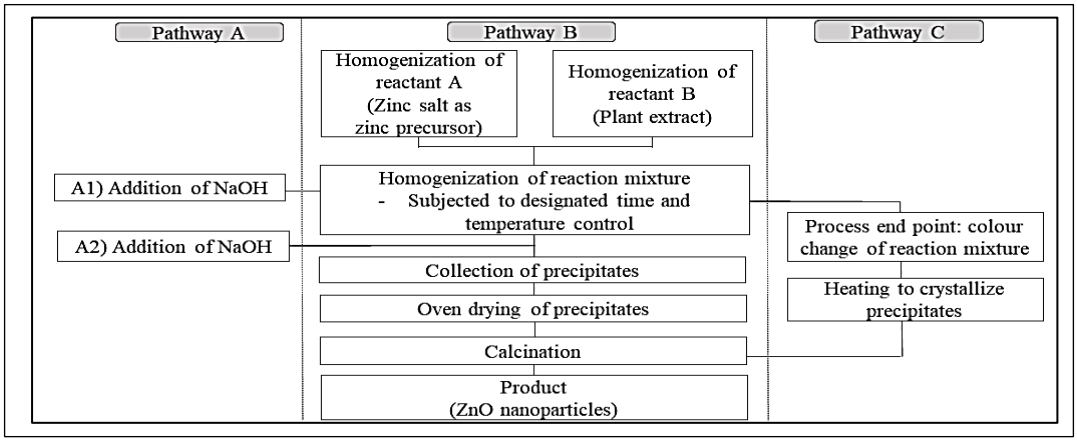

Figure 3. NaOH acts as alkalizing agent in pathway A1 and precipitating agent in pathway A2. Process endpoints of pathway A1, A2 and B are indicated by precipitation of zinc salts while that of pathway C is indicated by colour changes of reaction mixture.

Zinc oxide nanoparticles are formed in pathways B and C through the complexation of zinc with phytochemicals. The organic compounds are vaporized by calcining the zinc complexes. Based on the reaction mechanism, it is more precise to classify the phytochemicals as chelating agents rather than reducing agents. Since the mechanisms do not involve the nucleation and growth of ZnO particles, the nanoparticles produced should be smaller in size. However, the complexity of phytochemicals limits the repeatability of the pathway. Fluctuation in phytochemical quality would have a substantial impact on process yield and overall process duration.

Despite having a similar process flow with pathway B, pathway A2 requires the addition of NaOH at the end of synthesis. The acidity value (pKa) of the complex is determined by the acid-base properties of the ligand, where strong binding results in an increment of pKa [46]. A stable complex would precipitate at higher pH. The addition of NaOH is essential for the precipitation of Zn complexes after being subjected to a specific time and temperature control.

Present study employed pathway A1, which involved adding NaOH to the one-pot mixture of Zn precursor and plant extracts. The reducing properties of phytochemicals depend on their antioxidative activities. An antioxidant compound exhibits its properties via the hydrogen atom transfer (HAT) reaction and transfer reaction of a single electron (SET) [48]. Cited as reducing agents, the phytochemicals are favorable for their electron transfer tendency that would result in the formation of Lewis bases for Zn complexation. As per this study, deprotonated plant phenolic compounds were targeted as the main driving force in the formation of ZnO nanoparticles.

Depending on their pKa, phenolic compounds in liquid media exist as either weak acids or weak bases. Generally, the pKa of phenolic compounds lies between pH 8 and pH 10 [49]. When the pH of the surrounding falls below 8, the phenolic compounds exist as weak acids. Without the help of an alkalizing agent, a range of activation energies must be overcome for the –OH group of phenolic compounds to deprotonate. In present work, the addition of NaOH is crucial to accelerate the green synthesis of ZnO nanoparticles by aiding in phytochemical deprotonation.

In addition to assisting deprotonation of phytochemicals, an increase in reaction pH promotes the deprotonation of hydrated zinc complexes. This condition has a substantial effect on predominant species and the roles of phytochemicals. According to Krężel et al. [46], the deprotonation of hydrated zinc complexes begins at pH 7.8, and zinc hydroxo complexes predominate when the pH of the solution surpasses 8. The reaction ends at pH 11.8, with the final product being $[Zn(OH)_4]^{2-}$ complex [46]. Equations 1 – 4 represent the progression of hydrolysis and deprotonation.

$$[Zn(H_2O)_6]^{2+} + H_2O \rightleftharpoons [Zn(H_2O)_5(OH)]^{+} + H_3O^{+} \quad (1)$$

$$[Zn(H_2O)_5(OH)]^{+} + H_2O \rightleftharpoons [Zn(H_2O)_4(OH)_2] + H_3O^{+} \quad (2)$$

$$[Zn(H_2O)_4(OH)_2] + H_2O \rightleftharpoons [Zn(H_2O)_3(OH)_3]^{-} + H_3O^{+} \quad (3)$$

$$[Zn(H_2O)_3(OH)_3]^{-} + H_2O \rightleftharpoons [Zn(OH)_4]^{2-} + 2H_2O + H_3O^{+} \quad (4)$$

According to Krężel et al. [46], the precipitation of the uncharged $[Zn(H_2O)_4(OH)_2]$ results in the formation of an amorphous $Zn(OH)_2$ and five distinct types of $Zn(OH)_2$ crystals. The crystal forms of $Zn(OH)_2$ are unstable [46, 50], and their decomposition leads to the formation of ZnO nuclei. Meanwhile, $[Zn(OH)_4]^{2-}$ serves as growth template for the growth of ZnO nuclei in addition to decomposing into ZnO.

The pH profile of the reaction mixture reveals that the formation of ZnO nuclei occurs through the outlined mechanisms, with reaction mixtures A and B producing unstable $[Zn(OH)_4]^{2-}$ while reaction mixtures C, D, E, F, and G producing unstable $Zn(OH)_2$ crystals. According to LaMer's mechanism, this phase is critical for size control of ZnO nanoparticles since a high nucleation rate during a protracted reaction will result in the formation

of larger particles. This is evidenced by the fact that the particle sizes of ZnO generated from reaction mixtures A and B were larger than those of the other reaction mixtures. This reaction mechanism explained the effect of pH and NaOH concentration on the particle size of ZnO.

The roles of phytochemicals in green synthesis are inferred to be dependent on the reaction pH and the dominant species in the reaction mixture. In present study, the roles of phenolic compounds were defined with reference to particle sizes of green synthesized ZnO. When NaOH is added to the one-pot mixture, the role of phytochemicals as ligand bases for the formation of zinc complexes is expected to be diminished, while their role as capping agents, which stabilize the ZnO nuclei, becomes prominent under basic conditions. Nevertheless, increasing the pH of the solution would aid in the deprotonation of phenolic compounds [49]. Phenoxide ions could interact with the Zn hydroxo complexes to achieve ligand substitution. However, the role of phytochemicals as capping agents was more significant in this investigation, as demonstrated by the morphological differences between $ZnO_{control(A)}$ and $ZnO_{OPLE(B)}$. Meanwhile, when the concentration of NaOH used was relatively low, the involvement of phytochemicals as ligand bases for the formation of zinc complexes predominated in pathway A1. The condition was demonstrated by the decrement in particle sizes of ZnO as reaction pH was reduced. It is important to note that the addition of NaOH in pathway A1 does not negate the function of phytochemicals since deprotonation of phytochemicals is required for subsequent reactions.

In present study, phytochemicals and hydrated zinc complexes competed for NaOH to achieve deprotonation. Under basic conditions, the moiety rich in $[Zn(OH)_4]^{2-}$ complex ions will facilitate the growth of ZnO along the [0001] direction [50, 51]. In the meantime, the deprotonated phytochemicals with negative charges will be drawn to the Zn polar plane [0001], as well. A high concentration of $[Zn(OH)_4]^{2-}$ led to anisotropic growth and thus the formation of ZnO microflowers. As the concentration of $[Zn(OH)_4]^{2-}$ complex ions decreased, the adsorption of deprotonated phytochemicals on Zn polar plane became dominant.

The structure-directing effect of OPLE, as demonstrated by $ZnO_{OPLE(B)}$, could be attributed to its phytochemical complexity. It is speculated that the higher dosage of OPLE, which exhibited lower TPC, contributed to a higher content of amphiphilic phytochemicals in the aqueous plant extracts of green synthesis. This condition resulted in the isotropic growth of ZnO owing to the uniform adsorption by the phytochemicals.

Previously, the terms 'reducing agent', 'chelating agent', 'capping agent', and ‘structure-directing agent' were used interchangeably, and the definitions were ambiguous. Deprotonated phytochemical, which is a form of ligand base, is structurally a chelating agent when it interacts with either zinc hydroxo complexes or ZnO nuclei in the green synthesis. In the event that Zn complexes are formed, deprotonated phytochemicals shall be referred to as chelating agents; meanwhile, when deprotonated phytochemicals interact with ZnO nuclei to achieve electrostatic stabilization, they shall be defined as capping agents for precision. A structure-directing agent, on the other hand, possesses a structure-directing effect to control the growth of the nanoparticles [52]. It is illustrated in Figure 4 that nucleation and growth of ZnO nanoparticles occur via pathways A1 and A2, whereas the formation of Zn complexes occurs via pathways C and B.

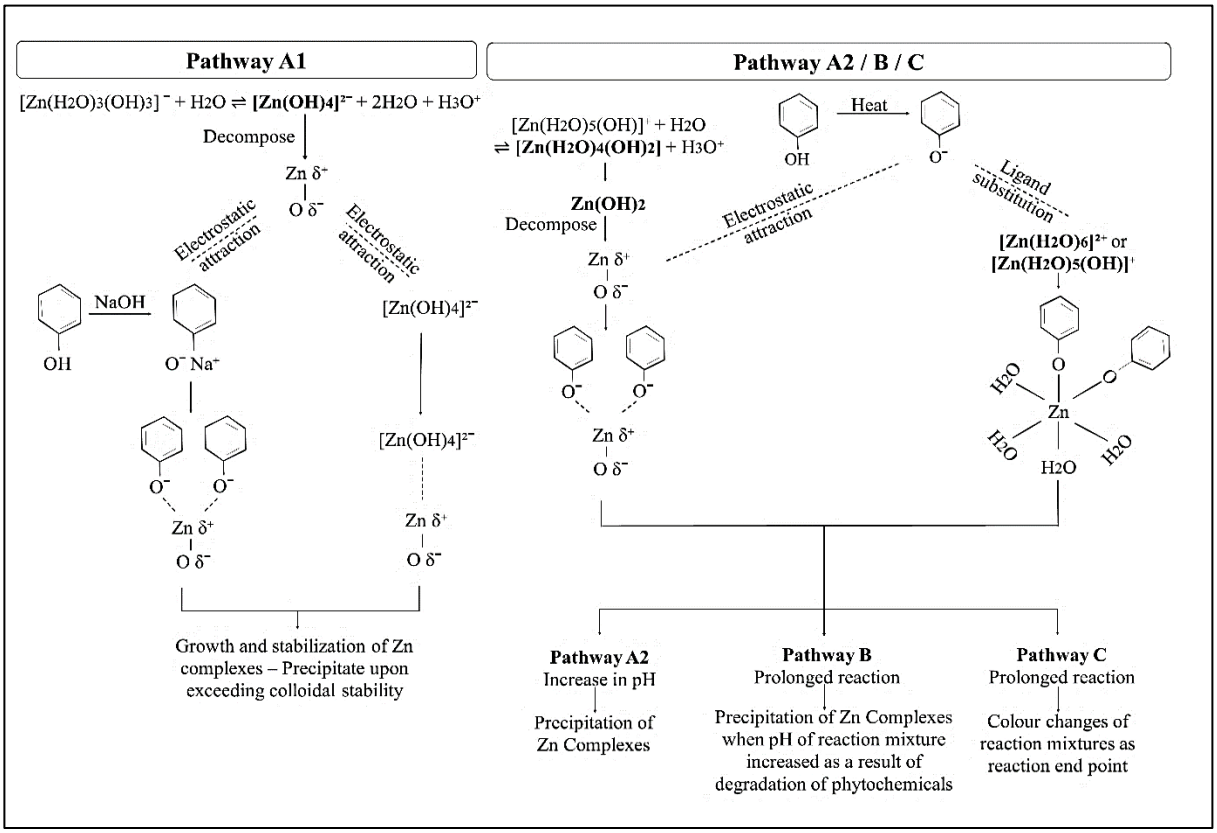

Figure 4. Deprotonated phytochemicals act primarily as capping agent when $[Zn(OH)_4]^{2-}$ is the predominant species while their roles as chelating agent are more prominent at neutral pH where Zn complexes are the predominant species.

Antibacterial strength of the green synthesized ZnO

Antibacterial activity of ZnO samples against *Staphylococcus aureus and Escherichia coli* was examined. There was a lack of antibacterial action against the latter. The minimum inhibitory concentration (MIC) of ZnO samples against *S. aureus* decreased with increasing ZnO particle size (Table 5). However, a slight dip was observed from $ZnO_{CLE(E)}$ to $ZnO_{CLE(F)}$. The condition was attributed to the colloidal stability of ZnO, which was dependent on the interplay of particle sizes and surface properties. It is worth noting that the antibacterial strength of ZnO synthesized through the incorporation of plant extracts ($ZnO_{BTLE(B)}$, $ZnO_{CLE(B)}$, and $ZnO_{OPLE(B)}$) were superior to that of $ZnO_{control(A)}$. In addition, the ZnO microstructures exhibited stronger antibacterial effects against *S. aureus* when compared to ampicillin and oxacillin. The two antibiotics showed no antibacterial activity when deployed at the same starting concentrations of 8 $mgmL^{-1}$ under the same experimental setup.

Table 5. Minimum inhibitory concentration of zinc oxide samples against *Staphylococcus aureus*

Reaction mixture	Minimum inhibitory concentration, mgmL^{-1}		
	ZnO_{BTLE}	**ZnO_{CLE}**	**ZnO_{OPLE}**
B	0.0313*	0.1250	0.1250*
C	0.2500*	0.2500	0.2500
D	1.0000	0.2500*	0.5000
E	1.0000	1.0000*	1.0000*
F	1.0000*	0.5000	2.0000*
G	2.0000	2.0000	2.0000*
A (control)		0.5000*	
Analytical grade ZnO		0.0625*	
Oxacillin		not effective	
Ampicillin		not effective	

*denotes minimum bactericidal concentration of ZnO samples

The antibacterial strength of ZnO microstructures had improved by at least fourfold when plant extracts were incorporated. Despite having similar morphologies, $ZnO_{BTLE(B)}$ and $ZnO_{CLE(B)}$ exhibited enhanced antibacterial effects against *S. aureus* than $ZnO_{control(A)}$. The capping of phytochemicals on the ZnO microstructures are speculated to have an additive effect on their antibacterial properties. However, no organic compounds were observed in the FTIR spectra of ZnO samples. This condition might be related to the method sensitivity, where particle size of samples negatively affected penetration depth of the IR light and intensity of bands the spectra [53].

Theoretically, the decrement in particle size would essentially enhance the antibacterial strength of nanoparticles since smaller particles have higher surface energy to aid in dissolution [54,55,56]. Raghupathi et al. [57] and Naqvi et al. [58] discovered the inversed relationship between particle size of ZnO and antibacterial activity against *S. aureus*. Contradictory to the theory, present studies found that the antibacterial strength against *S. aureus* reduced with a decrement in particle sizes, whereas ZnO with defined microstructures exhibited better antibacterial strength. It is speculated that the dissolution properties of nanoparticles might have contributed to the condition.

The dissolution of nanoparticles is affected by the chemistry of the administered condition, which includes ionic strength, pH, and temperature of the medium [59, 60]. The presence of dissolved organic matters would improve the colloidal stability of nanoparticles, which in turn reduces the rate of agglomeration [60, 61]. In the current investigation, however, ZnO samples and bacteria were suspended in sterile distilled water and 0.9 % saline. Peng et al. [60] reported that presence of inorganic ions would disrupt the electrostatic stability of nanoparticles. The presence of inorganic ions is speculated to be the factor contributing to the lack of ZnO nanoparticles' antibacterial action in present study.

The attack mechanisms of ZnO nanoparticles were theorized to be through the formation of ROS, cell internalization of abrasive ZnO, and the release of Zn^{2+} [9,62]. Despite being deployed at higher starting concentrations (16 mgmL^{-1}), ZnO samples and antibiotics had no antibacterial effect against *E. coli*. Meanwhile, Jin et al. [63] discovered that the UV irradiated spherical ZnO nanoparticles at 0.05 mgmL^{-1} had a remarkable activity against *E. coli*. The ZnO samples were used without any prior treatment in the present study. The absence of antibacterial activity against *E. coli* might be attributed to the incompatibility of attack mechanisms.

Based on these observations, it is postulated that the morphology of ZnO played a substantial role in its antibacterial properties against *S. aureus*. The abrasiveness and defined surface morphology of ZnO microstructures contribute to their improved antibacterial properties when compared to ZnO nanoparticles under the given experimental conditions. Meanwhile, the lack of antibacterial activity against *E. coli* might be due to the concentration-dependent effect of ZnO. Besides, the physical properties of ZnO microstructures and nanoparticles employed in this work are speculated to be incompatible with the target site of the tested strain of *E. coli*, making them incapable of exhibiting antibacterial activity.

Conclusion

The designed pathway is stable and repeatable for the green synthesis of ZnO nano- and micro- particles. Manipulation of total phenolic content is a feasible method to control concentration of incorporated plant extracts. The proposed synthesis pathway is feasible for size control of ZnO. Green synthesis is accelerated by the addition of NaOH where it assists deprotonation of phytochemicals to commence Zn chelation. Reaction pH influenced the roles of phytochemicals. The role of deprotonated phytochemicals as capping agent, which possesses structure-directing effect, is prominent under basic condition. Meanwhile, their role as chelating agent, which enhances particle size reduction, is prominent under neutral condition. In addition, it was deduced that the morphology of ZnO played a more substantial role in determining its antibacterial strength compared to particle size. In addition to quantitative phenolic profile, future studies are recommended to establish the interrelation between qualitative phytochemical profile of plant extracts and particle size of ZnO produced to improve universality of the green synthesis pathway.

Acknowledgement

This project is funded by the Ministry of Education Malaysia under the Consortium Research Grant Scheme (KKP) or KPM-special grant RMK10 with a reference number of KKP Vot No. K343. The authors would also like to thank Ministry of Higher Education Malaysia (MOHE) through Fundamental Research Grant Scheme (FRGS/1/2019/TK07/UTHM/02/1) and Universiti Tun Hussein Onn Malaysia which provide Graduate Research Grant Scheme (GPPS) under grant code H630 for sponsoring this work.

References

1. Inshakova, E. and Inshakov, O. (2017). World market for nanomaterials: structure and trends. *MATEC Web of Conferences,* 129: 02013.
2. Jeevanandam, J., Barhoum, A., Chan, Y. S., Dufresne, A. and Danquah, M. K. (2018). Review on nanoparticles and nanostructured materials: history, sources, toxicity and regulations. *Beilstein Journal of Nanotechnology,* 9: 1050-1074.
3. Singh, J., Dutta, T., Kim, K., Rawat, M., Samddar, P. and Kumar, P. (2018). 'Green' synthesis of metals and their oxide nanoparticles: applications for environmental remediation. *Journal of Nanobiotechnology,* 16: 84.
4. Zikalala, N., Matshetshe, K., Parani, S. and Oluwafemi, O. S. (2018). Biosynthesis protocols for colloidal metal oxide nanoparticles. *Nano-Struct. Nano-Objects,* 16: 288-299.
5. Kharissova, O. V., Kharisov, B. I., González, C. M. O., Méndez, Y. P. and López, I. (2019). Greener synthesis of chemical compounds and materials. *Royal Society Open Sciences,* 6: 191378.
6. Rodríguez-León, E., Rodríguez-Vázquez, B. E., Martínez-Higuera, A., Rodríguez-Beas, C., Larios-Rodríguez, E., Navarro, R. E., López-Esparza, R. and Iñiguez-Palomares, R. A. (2019). Synthesis of gold nanoparticles using *Mimosa tenuiflora* extract, assessments of cytotoxicity, cellular uptake, and catalysis. *Nanoscale Research Letters,* 14: 334.
7. Pal, S., Pal, K., Mukherjee, S., Bera, D., Karmakar, P. and Sukhen, D. (2020). Green cardamom mediated phytosynthesis of ZnO NPs and validation of its antibacterial and anticancerous potential. *Materials Research Express,* 7: 015068.

8. Soni, V., Raizada, P., Singh, P., Cuong, H. N., Rangabhashiyam, S., Saini, A., Saini, R. V., Le, Q. V., Nadda, A. K., Le, T. and Nguyen, V. (2021). Sustainable and green trends in using plant extracts for the synthesis of biogenic metal nanoparticles toward environmental and pharmaceutical advances: a review. *Environmental Research,* 202: 111622.
9. Siddiqi, K. S., Ur Rahman, A., Tajuddin and Husen, A. (2018). Properties of zinc oxide nanoparticles and their activity against microbes. *Nanoscale Research Letters,* 13(1): 141.
10. Pasquet, J., Chevalier, Y., Pelletier, J., Couval, E., Bouvier, D. A and Bolzinger, M. (2014). The contribution of zinc ions to the antimicrobial activity of zinc oxide. *Colloids Surface A Physicochemical Engineering Aspects,* 457: 263-274.
11. Król, A., Pomastowski, P., Rafińska, K., Railean-Plugaru, V. and Buszewski, B. (2017). Zinc oxide nanoparticles: synthesis, antiseptic activity and toxicity mechanism. *Advance Colloid Interface Sciences,* 249: 37-52.
12. Xu, J., Huang, Y., Zhu, S., Abbes, N., Jing, X. and Zhang, L. (2021). A review of the green synthesis of ZnO nanoparticles using plant extracts and their prospects for application in antibacterial textiles. *Journal Engineering Fibers Fabrication,* 16: 1-14.
13. Câmara, J. S., Albuquerque, B. R., Aguiar, J., Corrêa, R. C. G., Gonçalves, J. L., Granato, D., Pereira, J. A. M., Barros, L. and Ferreira, I. C. F. R. (2020). Food bioactive compounds and emerging techniques for their extraction: polyphenols as a case study. *Foods (Basel, Switzerland),* 10(1): 37.
14. Belščak-Cvitanović, A., Valinger, D., Benković, M, Tušek, A. J., Jurina, T., Komes, D. and Kljusurić, J. G. (2017). Integrated approach for bioactive quality evaluation of medicinal plant extracts using HPLC-DAD, spectrophotometric, near infrared spectroscopy and chemometric techniques. *International Journal Food Production,* 20(3): 1-18.
15. Almini, S. M. and Akbari, A. (2019). Metal nanoparticles synthesis through natural phenolic acids. *IET Nanobiotechnology,* 13(8): 771-777.
16. Mercado-Mercado, G., Blancas-Benitez, F. J., Velderrain-Rodríguez, G. R., Montalvo-González, E., González-Aguilar, G. A., Alvarez-Parrilla, E. and Sáyago-Ayerdi, S. G. (2015). Bioaccessibility of polyphenols released and associated to dietary fibre in calyces and decoction residues of Roselle (*Hibiscus sabdariffa* L.). *Journal Functional Foods,* 18: 171-181.
17. Dudonné, S., Vitrac, X., Coutière, P., Woillez, M. and Mérillon, J. (2009). Comparative study of antioxidant properties and total phenolic content of 30 plant extracts of industrial interest using DPPH, ABTS, FRAP, SOD, and ORAC assays. *Journal Agriculture Food Chemistry,* 57: 1768-1774.
18. Iqbal, E., Salim, K. A. and Lim, L. B. L. (2015). Phytochemical screening, total phenolics and antioxidant activities of bark and leaf extracts of *Goniothalamus velutinus* (Airy Shaw) from Brunei Darussalam. *Journal King Saud University Sciences,* 27: 224-232.
19. Gul, R., Jan, S. U., Faridullah, S., Sherani, S. and Jahan, N. (2017). Preliminary phytochemical screening, quantitative analysis of alkaloids, and antioxidant activity of crude plant extracts from *Ephedra intermedia* indigenous to Balochistan. *Science World Journal,* 2017: 5873648.
20. Aiyegoro, O. A. and Okoh, A. I. (2010). Preliminary phytochemical screening and *In vitro* antioxidant activities of the aqueous extract of *Helichrysum longifolium* DC. *BMC Complementary Alternative Medicine,* 10: 21.
21. Ukoha, P. O., Cemaluk, E. A. C., Nnamdi, O. L. and Madus, E. P. (2011). Tannins and other phytochemicals of the *Samanaea saman* pods and their antimicrobial activities. *African Journal Pure Applied Chemstry,* 5(8): 237-244.
22. El Aziz, M. M. A., Ashour, A. S. and Melad, A. S. G. (2019). A review on saponins from medicinal plants: chemistry, isolation, and determination. *Journal Nanomedicine Research,* 7(4): 282-288.
23. Shukla, S., Mehta, A. and Bajpai, V. K. (2013). Phytochemical screening and anthelmintic and antifungal activities of leaf extracts of *Stevia rebaudiana*. *Journal of Biologically Active Products from Nature,* 3(1): 56-63.

24. Top, A. and Çetinkaya, H. (2015). Zinc oxide and zinc hydroxide formation via aqueous precipitation: effect of the preparation route and lysozyme addition. *Materials Chemical Physics*, 167: 77-87.
25. He, Y., Ingudam, S., Reed, S., Gehring, A., Strobaugh, Jr. T. P. and Irwin, P. (2016). Study on the mechanism of antibacterial action of magnesium oxide nanoparticles against foodborne pathogens. *Journal Nanobiotechnology*, 14: 54.
26. Nandiyanto, A. B. D., Oktiani, R. and Ragadhita, R. (2019). How to read and interpret FTIR spectroscope of organic material. *Indonesian Journal Science Technology*, 4(1): 97-118.
27. Grasel, F. d. S., Ferrão, M. F. and Wolf, C. R. (2016). Development of methodology for identification the nature of the polyphenolic extracts by FTIR associated with multivariate analysis. *Spectrochimica Acta A Molecular Biomolecular Spectroscopy*, 153: 94-101.
28. Coates, J. (2006). Interpretation of infrared spectra, A practical approach. in R. A. Meyers and M. L. McKelvy (Ed.). *Encyclopedia of Analytical Chemistry*. Wiley, New York: pp. 10815-10837.
29. Santos, D. I., Correia, M. J. N., Mateus, M. M., Saraiva, J. A., Vicente, A. A. and Moldão, M. (2019). Fourier transform infrared (FT-IR) spectroscopy as a possible rapid tool to evaluate abiotic stress effects on pineapple by-products. *Applied Science*, 9: 4141.
30. Caunii, A., Pribac, G., Grozea, I., Gaitin, D. and Samfira, I. (2012). Design of optimal solvent for extraction of bio-active ingredients from six varieties of *Medicago sativa*. *Chemical Central Journal*, 6: 123.
31. Thummajitsakul, S., Samaikam, S., Tacha, S. and Silprasit, K. (2020). Study of FTIR spectroscopy, total phenolic content, antioxidant activity and anti-amylase activity of extracts and different tea forms of *Garcinia schomburgkiana* leaves. *LWT*, 134: 110005.
32. Baranska, M. and Schulz, H. (2009). Determination of alkaloids through infrared and Raman spectroscopy. in Cordell, G. A. (Ed.). *The Alkaloids: Chemistry and Biology*. Elsevier Inc., Netherlands: pp. 217-255.
33. Wahab, R., Kim, Y. and Shin, H. (2009). Synthesis, characterization and effect of pH variation on zinc oxide nanostructures. *Materials Transaction*, 50(8): 2092-2097.
34. Rayerfrancis, A., Bhargav, P. B., Ahmed, N., Chandra, B. and Dhara, S. (2015). Effect of pH on the morphology of ZnO nanostructures and its influence on structural and optic properties. *Physica B Condensation Matters*, 457: 96-102.
35. Rafaie, H. A., Samat, N. and Nor, R. M. (2014). Effect of pH on the growth of zinc oxide nanorods using *Citrus aurantifolia* extracts. *Materials Letters*, 137: 297-299.
36. Padalia, H., Moteriya, P. and Chanda, S. (2018). Synergistic antimicrobial and cytotoxic potential of zinc oxide nanoparticles synthesized using *Cassia auriculata* leaf extract. *BioNanoScience*, 8: 196-206.
37. Mohammadi, F. M. and Ghasemi, N. (2018). Influence of temperature and concentration on biosynthesis and characterization of zinc oxide nanoparticles using *cherry* extract. *Journal Nanostructure Chemistry*, 8: 93-102.
38. Suresh, J., Pradheesh, G., Alexramani, V., Sundrarajan, M. and Hong, S. I. (2018). Green synthesis and characterization of zinc oxide nanoparticles using insulin plant (*Costus pictus D. Don)* and investigation of its antimicrobial as well as anticancer activities. *Advance Nature Sciences: Nanoscience, Nanotechnology*, 9: 015008.
39. Umar, H., Kavaz, D. and Rizaner, N. (2019). Biosynthesis of zinc oxide nanoparticles using *Albizia lebbeck* stem bark, and evaluation of its antimicrobial, antioxidant, and cytotoxic activities on human breast cancer cell lines. *International Journal Nanomedicine*, 14: 87-100.
40. Sharmila, G., Thirumarimurugan, M. and Muthukumaran, C. (2019). Green synthesis of ZnO nanoparticles using *Tecoma castanifolia* leaf extract: characterization and evaluation of its antioxidant, bactericidal and anticancer activities. *Microchemical Journal*, 145: 578-587.

41. Matinise, N., Fuku, X. G., Kaviyarasu, K., Mayedwa, N. and Maaza, M. (2017). ZnO nanoparticles via *Moringa oleifera* green synthesis: physical properties & mechanism of formation. *Applied Surface Sciences,* 406: 339-347.
42. Fakhari, S., Jamzad, M. and Fard, H. K. (2019). Green synthesis of zinc oxide nanoparticles: a comparison. *Green Chemistry Letters Review*, 12(1): 19-24.
43. Liu, Y. C., Li, J., Ahn, J., Pu, J., Rupa, E. J., Huo, Y. and Yang, D. C. (2020). Biosynthesis of zinc oxide nanoparticles by one-pot green synthesis using fruit extract of *Amomum longiligulare* and its activity as a photocatalyst. *Optik*, 218: 165245.
44. Chakraborty, S., Farida, J. J., Simon, R., Kasthuri, S. and Mary, N. L. (2020). *Averrhoe carrambola* fruit extract assisted green synthesis of ZnO nanoparticles for the photodegradation of congo red dye. *Surface Interfaces,* 19: 100488.
45. Díaz, N., Suárez, D. and Merz, Jr. K. M. (2000). Hydration of zinc ions: theoretical study of $[Zn(H_2O)_4](H_2O)_8^{2+}$ and $[Zn(H_2O)_6](H_2O)_6^{2+}$. *Chemistry Physics Letters,* 326: 288-292.
46. Krężel, A. and Maret, W. (2016). The biological inorganic chemistry of zinc ions. *Archive Biochemical Biophysics,* 611: 3-19.
47. Soldatavić, T. (2018). Mechanism of interactions of zinc(II) and copper(II) complexes with small biomolecules. *IntechOpen*: pp. 79472.
48. Santos-Sánchez, N. F., Salas-Coronado, R., Villanueva-Cañongo, C. and Hernández-Carlos, B. (2019). Antioxidant compounds and their antioxidant mechanisms. *IntechOpen*: 85270.
49. Sobiesiak, M. (2017). Chemical structure of phenols and its consequence for sorption processes. *IntechOpen*: 66537.
50. Wang, M., Zhou, Y., Zhang, Y., Hahn, S. H. and Kim, E. J. (2011). From $Zn(OH)_2$ to ZnO: a study on the mechanism of phase transformation. *CrystEngComm,* 13: 6024-6026.
51. Zhu, Y. F., Fan, D. H., Dong, Y. W. and Zhou, G. H. (2014). Morphology-controllable ZnO nanostructures: ethanol-assisted synthesis, growth mechanism and solar cell applications. *Superlattices Microstructure,* 74*:* 261-272.
52. Javed, R., Zia, M., Naz, S., Aisida, S. O., Ain, N. U. and Ao, Q. (2020). Role of capping agents in the application of nanoparticles in biomedicine and environmental remediation: recent trends and future prospects. *Journal Nanobiotechnology,* 18: 172.
53. Udvardi, B., Kovács, I. J., Fancsik, T., Kónya, P., Bátori, M., Stercel, F., Falus G. and Szalai, Z. (2017). Effects of particle size on the attenuated total reflection spectrum of minerals. *Applied Spectroscopy,* 71(6): 1157-1168.
54. Peng, X., Palma, S., Fisher, N. S. and Wong, S. S. (2011). Effect of morphology of ZnO nanostructures on their toxicity to marine algae. *Aquatic Toxicology,* 102: 186-196.
55. Lallo da Silva, B., Abuçafy, M. P., Berbel Manaia, E., Oshiro Junior, J. A., Chiari-Andréo, B. G., Pietro, R. and Chiavacci, L. A. (2019). Relationship between structure and antimicrobial activity of zinc oxide nanoparticles: an overview. *International Journal Nanomedicine*, 14: 9395-9410.
56. Jin, S. and Jin, H. (2021). Antimicrobial activity of zinc oxide nano/microparticles and their combinations against pathogenic microorganisms for biomedical applications: from physicochemical characteristics to pharmacological aspects. *Nanomaterials (Basel, Switzerland),* 11(2): 263.
57. Raghupathi, K. R., Koodali, R. T. and Manna, A. C. (2011). Size-dependent bacterial growth inhibition and mechanism of antibacterial activity of zinc oxide nanoparticles. *Langmuir*, 27: 4020-4028.
58. Naqvi, Q., Kanwal, A., Qaseem, S., Naeem, M., Ali, S. R., Shaffique, M. and Maqbool, M. (2019). Size-dependent inhibition of bacterial growth by chemically engineered spherical ZnO nanoparticles. *Journal Biology Physics*, 45(2): 147-159.
59. Misra, S. K., Dybowska, A., Berhanu, D., Luoma, S. N. and Valsami-Jones, E. (2012). The complexity of nanoparticle dissolution and its importance in nanotoxicological studies. *Science Total Environment,* 438: 225-232.

60. Peng, Y., Tsai, Y., Hsiung, C., Lin, Y. and Shih, Y. (2017). Influence of water chemistry on the environmental behaviors of commercial ZnO nanoparticles in various water and wastewater samples. *Journal Hazardous Materials,* 322: 348-356.
61. Zhang, Y., Chen, Y., Westerhoff, P. and Crittenden, J. (2009). Impact of natural organic matter and divalent cations on the stability of aqueous nanoparticles. *Water Research*, 43: 4249-4257.
62. Dimapilis, E. A. S., Hsu, C., Mendoza, R. M. O. and Lu, M. (2018). Zinc oxide nanoparticles for water disinfection. *Sustainable Environmental Research,* 28: 47-56.
63. Jin, S., Jin, J., Hwang, W. and Hong, S. W. (2019). Photocatalytic antibacterial application of zinc oxide nanoparticles and self-assembled networks under dual UV irradiation for enhanced disinfection. *International Journal Nanomedicine,* 14: 1737-1751.